Giant Enhancement of the Optical Second-Harmonic Emission of WSe₂ Monolayers by Laser Excitation at Exciton Resonances

G. Wang, X. Marie, I. Gerber, T. Amand, D. Lagarde, L. Bouet, M. Vidal, A. Balocchi, and B. Urbaszek

Université de Toulouse, INSA-CNRS-UPS, LPCNO, 135 Avenue de Rangueil, 31077 Toulouse, France

We show that the light-matter interaction in monolayer WSe₂ is strongly enhanced when the incoming electromagnetic wave is in resonance with the energy of the exciton states of strongly Coulomb bound electron-hole pairs below the electronic band gap. We perform second harmonic generation (SHG) spectroscopy as a function of laser energy and polarization at $T = 4$ K. At the exciton resonance energies we record an enhancement by up to 3 orders of magnitude of the SHG efficiency, due to the unusual combination of electric dipole and magnetic dipole transitions. The energy and parity of the exciton states showing the strong resonance effects are identified in 1- and 2-photon photoluminescence excitation experiments, corroborated by first principles calculations. Targeting the identified exciton states in resonant 2-photon excitation allows us to maximize k-valley coherence and polarization.

Monolayers (MLs) of transition metal dichalcogenides (TMDC) such as WSe₂ and MoS₂ are an exciting class of two-dimensional (2D) materials for (opto-)electronics [1–7], nonlinear optics [8–13], and for exploring electron k-valley physics [14–16]. Crystal inversion symmetry breaking together with the spin-orbit interaction lead to a unique coupling of carrier spin and k-space valley physics [17–21], initially described in a single particle picture. When electrons and holes are simultaneously present, they will form excitons as the Coulomb interaction is enhanced by the strong quantum confinement, the large effective masses, and the reduced dielectric screening in these ideal 2D systems. Large exciton binding energies E_b of typically 0.5 eV are predicted [22–25] and have been confirmed experimentally very recently [26–31]; i.e., the energy of the lowest lying optical transition (optical band gap) is about 0.5 eV below the electronic band gap E_g.

In this work we demonstrate a variation over several orders of magnitude of the nonlinear and linear optical response of ML WSe₂. This is achieved by tuning the optical excitation *on* and *off* resonance with respect to the ground ($1s$) and excited ($2s, 2p...$) exciton states. At these particular energies, identified in 1- and 2-photon excitation spectroscopy, the light-matter interaction is strongly enhanced. We perform second harmonic generation (SHG) spectroscopy [32–34], i.e., we monitor the SHG signal as a function of laser energy and polarization. We find an enhancement of the SHG efficiency of up to 3 orders of magnitude when scanning the 2-photon laser energy across the excitonic spectrum of ML WSe₂, thereby determining the parity and energy of exciton states. Surprisingly, tuning the excitation laser in resonance with the $1s$ exciton states, for which 2-photon absorption is parity forbidden, results in strong SHG, as in addition to electric-dipole, also magnetic-dipole optical transitions

contribute to the frequency doubling [35]. Another important consequence of exciting the $2s$ or $2p$ exciton state resonantly is to maximize valley coherence and valley polarization in 2- and 1-photon absorption, providing an ideal starting point for valley index manipulation [15]. We evaluate the energy position of the electronic band gap E_g with respect to the excited exciton states with *ab initio* GW-Bethe Salpeter equation calculations [25,51].

We studied 1ML WSe₂ flakes obtained by micromechanical cleavage of bulk WSe₂ crystal (from 2D Semiconductors, USA) on 90 nm SiO₂ on a Si substrate. For 2-photon excitation we use *ps* pulses, generated by a tunable optical parametric oscillator (OPO) synchronously pumped by a mode-locked Ti:sapphire laser. Photoluminescence (PL) and SHG are collected in reflection geometry. For 1-photon excitation frequency doubled OPO pulses are used. In the experiments at $T = 4$ K the light is propagating perpendicular to the 2D layer plane; see Supplemental Material for details [35]. In standard PL experiments in Fig. 1(a) using excitation above the optical band gap we observe at 1.75 eV (FWHM ≈ 10 meV) the neutral A exciton (Coulomb bound electron-hole pair) and at 1.72 eV the charged exciton (trion) [52]. Under linearly polarized laser excitation, only the neutral exciton shows that linear polarization in emission as a coherent superposition of valley exciton states is created [52,53]. Figure 1(c) displays the results of 2-photon optical spectroscopy experiments performed for a linearly polarized excitation laser with energy $E_{laser} = 0.946$ eV, much lower than the optical gap of around 1.7 eV. Both the neutral exciton and the trion PL are observed at the same emission energy as for those above band gap excitation; compare Figs. 1(a) and 1(c). The spectrally narrow line at $E = 1.893$ eV $= 2 \times E_{laser}$ corresponds to the SHG in the WSe₂ ML; the spectral width is given by the ps laser pulse.
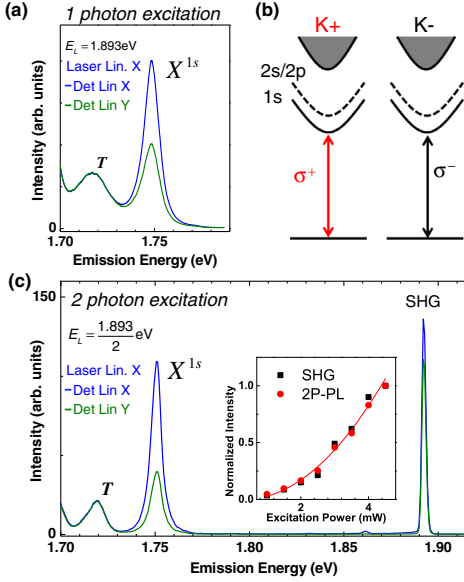
FIG. 1 (color online).   (a) Optical valley coherence generation following 1-photon absorption, linearly polarized (lin.X). The $1s$ state of the neutral A exciton and the trion (T) transitions are marked. PL spectra copolarized (cross) with the laser are shown in blue (green). The onset of the localized state emission can be seen at low energy. (b) 1-photon optical valley selection rules in the exciton representation for ML WSe$_2$. For simplicity, only the A-exciton series is shown. (c) Optical valley coherence generation following 2-photon absorption at $T = 4$ K. Inset: SHG intensity (squares) and 2-photon PLE (circles) as a function of laser power.

Both the A-exciton PL intensity following 2-photon absorption and the SHG intensity increase quadratically with the laser excitation power [see inset in Fig. 1(c)] [8–10], as expected for these nonlinear processes.

Second harmonic generation spectroscopy.— Broken inversion symmetry and strong light matter interaction make ML WSe$_2$ an ideal material for nonlinear optics. SHG generation at a *fixed* wavelength is commonly used for few layer TMDCs to probe crystal inversion symmetry [8–10]. In the experiment in Fig. 2(b), the intensity of the SHG signal is plotted as a function of the 2-photon laser excitation energy. Over the scanned range between 1.7 and 2.4 eV, we observe for all energies a measurable SHG signal. Strikingly, we observe a variation in SHG intensity over 3 orders of magnitude in Fig. 2(b), although the excitation power is kept constant in the experiments. Variations of a factor of ≈ 2 in SHG intensity have been reported for ML MoS$_2$ at 300 K as the laser is scanned across the $1s$ exciton resonance [11]. SHG intensity variations as a function of laser energy have also been reported in Malard *et al.* [12], albeit for laser energies well above the A- and B-exciton resonances.

A particularly surprising feature of these experiments is the strong SHG signal when the 2-photon laser energy is in resonance with $1s$ A exciton (1.75 eV) and the $1s$ B exciton (2.17 eV), whose energies were determined in the same

sample through PL and reflectivity [52]. In contrast to the SHG results, the $1s$ transitions are not observed in 2-photon PLE experiments, as demonstrated in Fig. 2(d), as they are dipole forbidden. PL emission and SHG can be clearly distinguished due to the different emission line-width and polarization selection rules; see Fig. S8 of the Supplemental Material [35]. The clear SHG resonances observed in Fig. 2(b) indicate therefore that contributions beyond the usual electric-dipole coupling of the light-matter interaction are involved. We have hence developed a theoretical description of the microscopic and macroscopic origins of SHG in ML TMDCs, see Supplemental Material [35]. Below we outline the key concepts:

The signal plotted in Fig. 2(b) is directly related to the nonlinear dielectric susceptibility tensor $\chi^{(2)}$ that can be evaluated with time dependent perturbation theory. As only very recently demonstrated for bulk ZnO, the efficiency of SHG depends not only on the symmetry of the crystal, but also on that of the exciton states [32,33]. Close to resonance of an excitonic state $|\Psi_{\text{exc}}\rangle$ we can write

$$\chi^{(2)}_{ijk}(-2\omega; \omega, \omega) \propto \langle \oslash | \hat{V}^{2\omega}_i \frac{|\Psi_{\text{exc}}\rangle \langle \Psi_{\text{exc}}|}{E_{\text{exc}} - 2\omega\hbar - i\Gamma_{\text{exc}}}$$
$$\times \hat{V}^{\omega}_j \sum_{\text{vi}} \frac{|\Psi_{\text{vi}}\rangle \langle \Psi_{\text{vi}}|}{E_{\text{vi}} - \omega\hbar - i\Gamma_{\text{vi}}} \hat{V}^{\omega}_k |\oslash\rangle. \quad (1)$$

Here, $|\oslash\rangle$ is the ground state, $|\Psi_{\text{vi}}\rangle$ the virtual intermediate state, and $|\Psi_{\text{exc}}\rangle$ the excitonic state. The term with $E_{\text{exc}} - 2\omega\hbar - i\Gamma_{\text{exc}}$ is dominant over similar terms obtained in the summation over all possible virtual exciton states, as for a real, excitonic state the damping $\Gamma_{\text{exc}} \ll \Gamma_{\text{vi}}$ as it lives longer than a virtual state. The tensor components (i, j, k) may belong to the $+, -, 0$ standard set, where $+(-)$ correspond to right (left) circularly polarized components and 0 to z-polarized ones, z is perpendicular to the ML. To go beyond the electric dipole approximation, the exciton-photon is expanded as

$$\hat{V}^{\omega}_i = \hat{V}^{\text{ED}}_i(\omega) + \hat{V}^{\text{QE}}_i(\omega) + \hat{V}^{\text{MD}}_i(\omega) + \text{H.c.} \quad (2)$$

The matrix element corresponding to the electric quadrupole (QE) interaction vanishes in ML WSe$_2$ for symmetry reasons [35], in contrast to bulk ZnO. We can write the remaining 2 interactions, namely, the electric (ED) and magnetic dipole (MD) interactions for pure $\sigma^{\pm}$ circularly polarized light as

$$\hat{V}^{\text{ED}}_{\pm} = -i\frac{\mathcal{E}_0}{4m_0 c} e^{i\omega t}(\hat{p}_x \pm i\hat{p}_y), \quad (3)$$

$$\hat{V}^{\text{MD}}_{\pm} = i\frac{\mathcal{B}_0}{2m_0} e^{i\omega t}\hat{L}_{\pm}, \quad (4)$$

where $q_z = q = \omega/c$ and $\mathcal{B}_0 = \mathcal{E}_0/c$. It can be seen that the MD and the ED interactions are never in competition for a
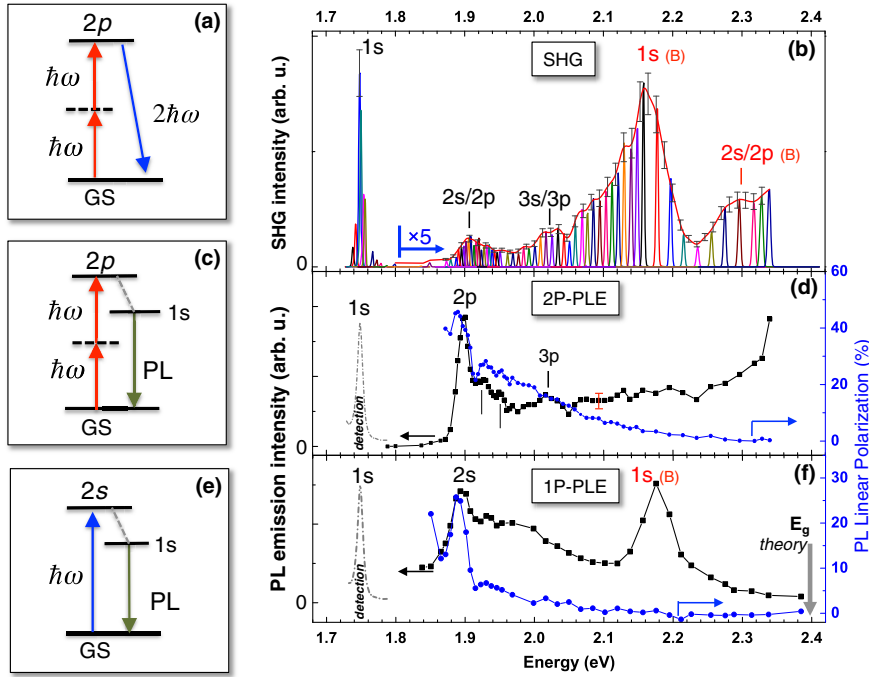
FIG. 2 (color online). (a) Schematic for SHG when 2 incident photons are resonant with the $2p$ state of the A exciton (b) results of SHG spectroscopy at $T = 4$ K as a function of $2\hbar\omega$. Typical error bars are shown, based on the standard deviation of the measured laser pulse width (for each wavelength) as a direct measure of the fluctuation of the peak power during the experiment. (c) Schematic for 2-photon PLE, (d) 2-photon PLE intensity (left axis, black squares), and linear polarization (right axis, blue circles) as a function of $2\hbar\omega$. Typical error bar indicated (e) schematic for 1-photon PLE (f), 1-photon PLE intensity (left axis, black squares), and linear polarization (right axis, blue circles) as a function of $\hbar\omega$.

given transition, but are complementary to each other, due to distinctly different symmetry and angular momentum selection rules. We identify as the most efficient SHG sequences governed by Eq. (1) processes that involve two ED and, very importantly, one MD transition. This explains the strong SHG that is observed at the $1s$ A-exciton resonance: First the MD interaction couples the ground state $|\oslash\rangle$ to a virtual $2p$ state. Second, the $2p$ state can be coupled to the $1s$ state via the ED interaction. Finally, the ED interaction couples the $1s$ virtual state back to the ground state $|\oslash\rangle$, giving rise to the SHG signal. In similar fashion, the ground state can couple to the $2p$ A exciton via two ED transitions (energy $\hbar\omega$), and the SHG signal is emitted via the MD interaction, as shown in Fig. 2(a) [35]. Efficient SHG generation involving relatively weak MD transitions (by typically 2 orders of magnitude compared to ED) comes from the presence of energetically well-defined excitonic resonances in ML WSe_2 with finite damping Γ_{exc}, as can be seen from Eq. (1), explaining the sharp SHG resonances with FWHM very similar to the exciton emission; compare Figs. 2(b) and 1(a).

In addition to the $1s$ A and B excitons, we observe clear resonances at 1.9, 2.03, and above 2.31 eV. To clarify the exact origin of these transitions and to investigate their excitonic nature and their symmetry, we perform in addition to SHG spectroscopy 2-photon and 1-photon PL excitation experiments.

Two-photon PLE experiments.— In 2-photon PL excitation (2P-PLE) experiments, the exciton states with p symmetry can be directly addressed [26,30], assuming the usual ED interaction is dominant. In the experiment, the laser power is kept constant and the detection energy is set to the emission peak of the $1s$ A exciton. The PL intensity

as a function of the 2-photon laser excitation energy is plotted in Fig. 2(d) (left axis), the linear polarization degree, corresponding to valley coherence, of the $1s$ A-exciton PL is also plotted (right axis); see Fig. S5 of the circular polarization degree [35]. Starting the 2P-PLE just above the $1s$ emission energy, we observe a first clear peak at 1.898 eV, as in SHG spectroscopy. Absorption for the ns A excitons is forbidden by the 2-photon ED section rules, so we assign this peak to the $2p$ state, 140 meV above the $1s$ exciton emission [54]. As for SHG spectroscopy, we observe in 2P-PLE a small peak at 2.03 eV, which we tentatively assign to the $3p$ state. In 2-photon PLE, we do not observe the $1s$ B exciton, in agreement with ED selection rules. Also, taking the trion emission as a measure for $1s$ exciton generation, we find that resonant 2-photon excitation of the $2p$ state results in strong trion emission, whereas resonant 2-photon excitation of the $1s$ state results in negligible trion emission. This observation is consistent with the assumption that 2-photon excitation of the $1s$ state is only allowed combining one ED and one MD transition, and not via two ED transitions.

One-photon PLE spectroscopy.— The findings from the two polarization resolved nonlinear optical techniques are further complemented by 1-photon optical spectroscopy, giving access to the s-exciton states whereas the p states are forbidden. Figure 2(f) displays the 1-photon PL excitation (1P-PLE) results. A clear peak corresponding to the $2s$ A exciton is observed at ≈ 1.9 eV, 140 meV above X_A^{1s}. Comparing the results of 1P-PLE and 2P-PLE in Figs. 2(d) and 2(f) we can infer that the $2s$ and $2p$ A-exciton states have the same energy within the spectral resolution of our excitation spectra (which is of the order of meV) [57,58].

Efficient generation of exciton valley coherence follow-ing 2-photon absorption.— A key argument for the attribution of the observed maxima in PLE following 1- and 2-photon absorption to excitonic states comes from the polarization dependence plotted in Figs. 2(d) and 2(f). Following excitation with linearly polarized light, the $1s$ A-exciton emission is strongly linearly polarized [59]. When the 2-photon laser is in resonance with the $2p$ state, we observe a global maximum of the linear polarization of 45%. In contrast to the exciton spin coherence observed for resonant excitation of GaAs quantum wells [60,61], the linear exciton polarization in ML TMDC probes the coherence arising from excitons from two different valleys in k space [53]. Our measurements indicate that the valley coherence is stronger when the $2p$ exciton state is directly photogenerated compared to the situation of the photogeneration of a hot $1s$ exciton state at the same energy. This most likely results from efficient intraexciton energy relaxation $2p \to 1s$ preserving the initially created coherent superposition of states. The results presented in Fig. 2(d) demonstrate for the first time in a semiconductor that significant exciton pseudospin coherence can be created with a 2-photon process. Two-photon excitation ($E_{\text{Laser}} \ll E_g$) does not generate excess carriers via non-excitonic absorption channels, which is beneficial for long valley coherence times. Also in 1-photon PLE we find a clear enhancement of the observed valley coherence when the laser is in resonance with the $2s$ exciton [62]. Also the valley polarization, monitored through the circular polari-zation degree, is enhanced when the $2s$ and $2p$ exciton states are addressed resonantly; see Fig. S5 [35]. Note that the resonance at 1.9 eV observed in SHG in Fig. 2(d) can be attributed to contributions coming from both the $2s$ and $2p$ exciton transitions, identified via intensity and polarization analysis in 2-photon [Fig. 2(d)] and 1-photon [Fig. 2(f)] PLE. The difference between the $1s$ and $2s/2p$ A-exciton states is 140 meV and we also observe a resonance 140 meV above the $1s$ B exciton, that we tentatively assign to the $2s/2p$ of the B exciton.

Exciton levels in ML TMDCs.— The three complementary experimental techniques presented in Figs. 2(b), 2(d), and 2(f) have uncovered the excited exciton states $2s$, $2p$, and $3p$. Their energy spacing is similar to the values reported at $T = 300$ K in the same material system [26]. In the absence of a clear signature of the electronic band gap E_g in our low temperature experiments, we have calculated E_g. The vertical arrow labeled $E_g = 2.37$ eV is the quasiparticle gap in Fig. 3 calculated at the GW_0 level including spin-orbit coupling, with typical error bars of ± 200 meV for this method [28], which we deduce from calculations with different parameter settings. If we define the exciton binding energy as $E_g - E(X_A^{1s}) = E_b$ we can roughly estimate $E_b = 600 \pm 200$ meV; see more details in [35]. As He *et al.* [26] determined $E_b \approx 370$ meV at $T = 300$ K in ML WSe$_2$, our theory seems to overestimate E_g. In general a
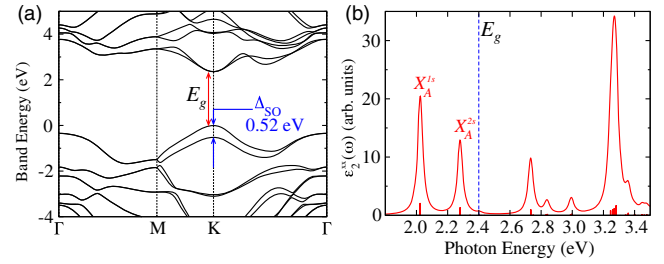

FIG. 3 (color online). (a) Quasiparticle band structure of WSe$_2$ monolayer at the GW_0 level, including spin-orbit coupling perturbatively. (b) Frequency dependent imaginary part of the transverse dielectric function including excitonic effects and oscillator strengths of the optical transitions (bars), calculated at the BSE-GW_0 level without spin-orbit coupling. The corre-sponding GW_0 gap ($E_g = 2.4 \pm 0.2$ eV) is also indicated.

high E_b is consistent with (a) the measured charged exciton binding energy in Figs. 1(a) and 1(c) where $E_b(\text{trion}) = 35$ meV [63,64] in this sample and (b) the values reported for E_b by other groups in ML TMDC [26–31]. Our GW calculations also show the existence of at least one excited exciton state labeled $2s$ in Fig. 3(b). We confirm a strong deviation of the standard 2D Rydberg series, for which two possible explanations have been suggested: (i) The strength of the effective Coulomb interaction will be very different for $1s$ and $2s$ states, for example, due to the strong variation of the effective dielectric constant as a function of the spatial extension of the exciton state [65,66]; (ii) using the formal-ism of relativistic quantum mechanics, strong Coulomb coupling leading in extreme cases to an excitonic collapse, as observed recently for artificial nuclei on graphene [67], has been predicted for ML TMDCs [68,69]. This would lead to very different optical selection rules and we hope our detailed investigation in 1- and 2-photon experiments pro-vides helpful experimental input for verifying these pre-dictions. Both (i) and (ii) critically depend on the dielectric environment of the substrate; here more systematic studies using suspended samples and different substrates are needed.

In summary, we have measured the spectral dependences of both the first order dielectric susceptibility (1-photon PLE) and the second order dielectric susceptibility (SHG excitation spectra for its real part and 2-photon PLE for its imaginary part). These experiments directly demonstrate that excitonic effects enhance the linear and nonlinear optical response of ML WSe$_2$ by several orders of magnitude and reveal that the valley coherence can be achieved following 2-photon excitation.

[1] A. K. Geim and I. V. Grigorieva, Nature (London) **499**, 419 (2013).

[2] S. Z. Butler, S. M. Hollen, L. Cao, Y. Cui, J. A. Gupta, H. R. Gutirrez, T. F. Heinz, S. S. Hong, J. Huang, A. F. Ismach et al., ACS Nano **7**, 2898 (2013).

[3] W. Zhao, Z. Ghorannevis, L. Chu, M. Toh, C. Kloc, P.-H. Tan, and G. Eda, ACS Nano **7**, 791 (2013).

[4] K. F. Mak, C. Lee, J. Hone, J. Shan, and T. F. Heinz, Phys. Rev. Lett. **105**, 136805 (2010).

[5] A. Splendiani, L. Sun, Y. Zhang, T. Li, J. Kim, C.-Y. Chim, G. Galli, and F. Wang, Nano Lett. **10**, 1271 (2010).

[6] B. Radisavljevic, A. Radenovic, J. Brivio, V. Giacometti, and A. Kis, Nat. Nanotechnol. **6**, 147 (2011).

[7] J. S. Ross, P. Klement, A. M. Jones, N. J. Ghimire, J. Yan, D. G. Mandrus, T. Taniguchi, K. Watanabe, K. Kitamura, W. Yao et al., Nat. Nanotechnol. **9**, 268 (2014).

[8] N. Kumar, S. Najmaei, Q. Cui, F. Ceballos, P. M. Ajayan, J. Lou, and H. Zhao, Phys. Rev. B **87**, 161403 (2013).

[9] H. Zeng, G.-B. Liu, J. Dai, Y. Yan, B. Zhu, R. He, L. Xie, S. Xu, X. Chen, W. Yao, and X. Cui, Sci. Rep. **3**, 1608 (2013).

[10] Y. Li, Y. Rao, K. F. Mak, Y. You, S. Wang, C. R. Dean, and T. F. Heinz, Nano Lett. **13**, 3329 (2013).

[11] X. Yin, Z. Ye, D. A. Chenet, Y. Ye, K. OBrien, J. C. Hone, and X. Zhang, Science **344**, 488 (2014).

[12] L. M. Malard, T. V. Alencar, A. P. M. Barboza, K. F. Mak, and A. M. de Paula, Phys. Rev. B **87**, 201401 (2013).

[13] M. L. Trolle, G. Seifert, and T. G. Pedersen, Phys. Rev. B **89**, 235410 (2014).

[14] D. Xiao, M.-C. Chang, and Q. Niu, Rev. Mod. Phys. **82**, 1959 (2010).

[15] K. F. Mak, K. L. McGill, J. Park, and P. L. McEuen, Science **344**, 1489 (2014).

[16] X. Xu, D. Xiao, T. F. Heinz, and W. Yao, Nat. Phys. **10**, 343 (2014).

[17] D. Xiao, G.-B. Liu, W. Feng, X. Xu, and W. Yao, Phys. Rev. Lett. **108**, 196802 (2012).

[18] T. Cao, G. Wang, W. Han, H. Ye, C. Zhu, J. Shi, Q. Niu, P. Tan, E. Wang, B. Liu et al., Nat. Commun. **3**, 887 (2012).

[19] K. F. Mak, K. He, J. Shan, and T. F. Heinz, Nat. Nanotechnol. **7**, 494 (2012).

[20] G. Sallen, L. Bouet, X. Marie, G. Wang, C. R. Zhu, W. P. Han, Y. Lu, P. H. Tan, T. Amand, B. L. Liu et al., Phys. Rev. B **86**, 081301 (2012).

[21] H. Zeng, J. Dai, W. Yao, D. Xiao, and X. Cui, Nat. Nanotechnol. **7**, 490 (2012).

[22] T. Cheiwchanchamnangij and W. R. L. Lambrecht, Phys. Rev. B **85**, 205302 (2012).

[23] H.-P. Komsa and A. V. Krasheninnikov, Phys. Rev. B **86**, 241201 (2012).

[24] A. Ramasubramaniam, Phys. Rev. B **86**, 115409 (2012).

[25] D. Y. Qiu, F. H. da Jornada, and S. G. Louie, Phys. Rev. Lett. **111**, 216805 (2013).

[26] K. He, N. Kumar, L. Zhao, Z. Wang, K. F. Mak, H. Zhao, and J. Shan, Phys. Rev. Lett. **113**, 026803 (2014).

[27] A. R. Klots, A. K. M. Newaz, B. Wang, D. Prasai, H. Krzyzanowska, D. Caudel, N. J. Ghimire, J. Yan, B. L. Ivanov, K. A. Velizhanin et al., Sci. Rep. **4**, 6608 (2014).

[28] M. M. Ugeda, A. J. Bradley, S.-F. Shi, F. H. da Jornada, Y. Zhang, D. Y. Qiu, S.-K. Mo, Z. Hussain, Z.-X. Shen, F. Wang et al., Nat. Mater. **13**, 1091 (2014).

[29] A. Chernikov, T. C. Berkelbach, H. M. Hill, A. Rigosi, Y. Li, O. B. Aslan, D. R. Reichman, M. S. Hybertsen, and T. F. Heinz, Phys. Rev. Lett. **113**, 076802 (2014).

[30] Z. Ye, T. Cao, K. O'Brien, H. Zhu, X. Yin, Y. Wang, S. G. Louie, and X. Zhang, Nature (London) **513**, 214 (2014).

[31] B. Zhu, X. Chen, and X. Cui, arXiv:1403.5108.

[32] D. C. Haueisen and H. Mahr, Phys. Rev. Lett. **26**, 838 (1971).

[33] M. Lafrentz, D. Brunne, A. V. Rodina, V. V. Pavlov, R. V. Pisarev, D. R. Yakovlev, A. Bakin, and M. Bayer, Phys. Rev. B **88**, 235207 (2013).

[34] H. Ito, F. Minami, K. Yoshida, and K. Inoue, J. Lumin. **66–67**, 493 (1995).

[35] See Supplemental Material at http://link.aps.org/supplemental/10.1103/PhysRevLett.114.097403, which contains additional references [36–50] on computational details, SHG and 2-photon selection rules, and exciton-phonon interaction.

[36] E. L. Ivchenko and G. Pikus, Superlattices and other Heterostructures, Symmetry and Optical Phenomena, Springer Series in Solid State Science 110 (Springer Verlag, Berlin, Heildelberg, 1995).

[37] G. F. Koster, J. O. Dimmock, G. Wheeler, and R. G. Satz, Properties of Thirty-Two Point Groups (M.I.T. Press, Cambridge, MA, 1963).

[38] M. M. Glazov, T. Amand, X. Marie, D. Lagarde, L. Bouet, and B. Urbaszek, Phys. Rev. B **89**, 201302 (2014).

[39] A. Yariv and P. Yeh, Optical Waves in Crystals, Propagation and Control of Laser Radiation, Wiley Series in Pure and Applied Optics (John Wiley and Sons, New York, 1984).

[40] C. Cohen-Tannoudji, B. Diu, and F. Laloe, Quantum Mechanics, Wiley Interscience Publications (Wiley and Sons, New York and Hermann, Paris, 1977).

[41] G. Kresse and J. Hafner, Phys. Rev. B **47**, 558 (1993).

[42] G. Kresse and J. Furthmuller, Comput. Mater. Sci. **6**, 15 (1996).

[43] J. P. Perdew, K. Burke, and M. Ernzerhof, Phys. Rev. Lett. **77**, 3865 (1996).

[44] P. E. Blöchl, Phys. Rev. B **50**, 17953 (1994).

[45] G. Kresse and D. Joubert, Phys. Rev. B **59**, 1758 (1999).

[46] M. Shishkin and G. Kresse, Phys. Rev. B **74**, 035101 (2006).

[47] A. A. Mostofi, J. R. Yates, Y.-S. Lee, I. Souza, D. Vanderbilt, and N. Marzari, Comput. Phys. Commun. **178**, 685 (2008).

[48] C. Franchini, R. Kovacik, M. Marsman, S. S. Murthy, J. He, C. Ederer, and G. Kresse, J. Phys. Condens. Matter **24**, 235602 (2012).

[49] F. Hüser, T. Olsen, and K. S. Thygesen, Phys. Rev. B **88**, 245309 (2013).

[50] A. Molina-Sanchez, D. Sangalli, K. Hummer, A. Marini, and L. Wirtz, Phys. Rev. B **88**, 045412 (2013).

[51] G. Onida, L. Reining, and A. Rubio, Rev. Mod. Phys. **74**, 601 (2002).

[52] G. Wang, L. Bouet, D. Lagarde, M. Vidal, A. Balocchi, T. Amand, X. Marie, and B. Urbaszek, Phys. Rev. B **90**, 075413 (2014).

[53] A. M. Jones, H. Yu, N. J. Ghimire, S. Wu, G. Aivazian, J. S. Ross, B. Zhao, J. Yan, D. G. Mandrus, D. Xiao et al., Nat. Nanotechnol. **8**, 634 (2013).

[54] The $2p$ A-exciton absorption shows two secondary peaks located 30 and 60 meV above the $2p$ main exciton peak, which correspond to enhanced PL when the laser energy corresponds to $X_A^{2p} + E_{phonon}$ and $X_A^{2p} + 2E_{phonon}$. Raman studies identified two optical phonon modes with energy of about $E_{phonon} = 31$ meV(250 cm^{-1}) in WSe2 ML; see [35] for details [55,56].

[55] H. Li, G. Lu, Y. Wang, Z. Yin, C. Cong, Q. He, L. Wang, F. Ding, T. Yu, and H. Zhang, Small **9**, 1974 (2013).

[56] H. Sahin, S. Tongay, S. Horzum, W. Fan, J. Zhou, J. Li, J. Wu, and F. M. Peeters, Phys. Rev. B **87**, 165409 (2013).

[57] R. L. Greene, K. K. Bajaj, and D. E. Phelps, Phys. Rev. B **29**, 1807 (1984).

[58] L. Vina, R. T. Collins, E. E. Mendez, and W. I. Wang, Phys. Rev. Lett. **58**, 832 (1987).

[59] In contrast to the coherent exciton alignment with the excitation laser polarization, the SHG emission as a function of the laser polarization angle is simply given by the underlying lattice symmetry [8–10]; see [35].

[60] S. Bar-Ad and I. Bar-Joseph, Phys. Rev. Lett. **66**, 2491 (1991).

[61] X. Marie, P. Le Jeune, T. Amand, M. Brousseau, J. Barrau, M. Paillard, and R. Planel, Phys. Rev. Lett. **79**, 3222 (1997).

[62] Note that the experiments on optical generation of excitonic valley coherence in ML WSe$_2$ recently published [53] use a 1-photon laser energy which coincides exactly with the $2s$ exciton absorption identified in our work.

[63] A. Thilagam, Phys. Rev. B **55**, 7804 (1997).

[64] K. F. Mak, K. He, Changgu, G. H. Lee, J. Hone, T. F. Heinz, and J. Shan, Nat. Mater. **12**, 207 (2013).

[65] P. Cudazzo, I. V. Tokatly, and A. Rubio, Phys. Rev. B **84**, 085406 (2011).

[66] J. Deslippe, M. Dipoppa, D. Prendergast, M. V. O. Moutinho, R. B. Capaz, and S. G. Louie, Nano Lett. **9**, 1330 (2009).

[67] Y. Wang, D. Wong, A. V. Shytov, V. W. Brar, S. Choi, Q. Wu, H.-Z. Tsai, W. Regan, A. Zettl, R. K. Kawakami, S. G. Louie, L. S. Levitov, and M. F. Crommie, Science **340**, 734 (2013).

[68] A. S. Rodin and A. H. Castro Neto, Phys. Rev. B **88**, 195437 (2013).

[69] T. Stroucken and S. W. Koch, arXiv:1404.4238.